Rock Mechanics and Rock Engineering (2019) 52:1247–1256
https://doi.org/10.1007/s00603-018-1659-y

TECHNICAL NOTE

Residual Strength Characteristics of CJPL Marble Under True Triaxial Compression

Zhi Zheng[1,3] · Xia-Ting Feng[2] · Xiwei Zhang[2] · Jun Zhao[2] · Cheng-Xiang Yang[2]

Received: 28 June 2018 / Accepted: 12 November 2018 / Published online: 27 November 2018

Keywords True triaxial compression · Residual strength · Deformation-dependence · Intermediate principal stress effect · Acoustic emission

1 Introduction

After excavation of underground caverns and tunnels, surrounding rocks suffer the development of the excavation damaged zone (EDZ), which still exhibits a certain bearing capacity (Hudson 1989; Hoek et al. 1995; Kaiser 2016). The studies of post-peak characteristics and residual strength play a crucial role in evaluating the bearing capacity (Cai et al. 2007a, b; Gao and Kang 2017). In recent decades, research on residual strength has made great progress and this has exerted a profound influence on the optimal design of supporting structures (Peng et al. 2017). However, the China Jinping Underground Laboratory Phase II (CJPL-II, with a burial depth of about 2400 m) is constructed under a state of three-dimensional (3D) high-geostress (Feng et al. 2018). The residual strength characteristics in this 3D stress state are not yet clear [e.g., the influence of intermediate principal stress (σ_2)], which deserved to be explored further.

There has been considerable research on the complete stress–strain curve of rock obtained by uniaxial or conventional triaxial laboratory tests ($\sigma_2=\sigma_3$) (Wawersik and Brace 1971; Hudson et al. 1972; Liao and Hsieh 1999; Labuz and Dai 2000; Hashiba et al. 2006; Barla et al. 2010; Peng et al. 2017), which provide a basis for investigating residual strength. Based on these data, the residual strength characteristics of rock have been studied and described by some strength criteria and models. Some scholars have researched the relationship between residual strength and confining pressure using existing 2D strength criteria. The linear relationship was studied by Mohr–Coulomb criterion (Cai et al. 2007a, b; Yang et al. 2012) and the non-linear relationship was explored by Hoek–Brown (Cai et al. 2007a; Gao and Kang 2017) and a second-order polynomial function (Joseph 2000). Others (Fang and Harrison 2001; Zhang et al. 2010) proposed a reduction index to convert peak strength to residual strength, which was related to confining pressure. By taking peak strength, confining pressure, and plastic deformation as variables, others (Kaiser 2016; Peng et al. 2017) have established a mobilised post-peak strength model, which could predict the residual strength of rock at sufficient strain: however, the aforementioned two models describe peak strength by using 2D criteria, thus still investigating the relationship between residual strength and confining pressure.

With redistribution of 3D stresses after underground cavern excavation, σ_3 and σ_2 change non-synchronously. The aforementioned residual strength data under uniaxial and conventional triaxial compression ($\sigma_2=\sigma_3$) fail to evaluate contributions of independent σ_3, let alone the influence of σ_2. A true triaxial system can be used to investigate the aforementioned topic theoretically. However, true triaxial tests are mainly carried out to study peak strength characteristics, strength criteria (Mogi 1971; Al-Ajmi and Zimmerman 2005), failure-plane angle (Mogi 1973; Ma and Haimson 2016), and other aspects such as unloading-induced spalling and rockburst (He et al. 2015, Su et al. 2017; Li et al. 2018), etc. The literature on post-peak behaviour of rock remains sparse with regard to provision of residual strength data in 3D stress states.

✉ Xia-Ting Feng
xtfeng@whrsm.ac.cn; xia.ting.feng@gmail.com

[1] State Key Laboratory of Geomechanics and Geotechnical Engineering, Institute of rock and Soil Mechanics, Chinese Academy of Sciences, Wuhan 430071, China

[2] Key Laboratory of Ministry of Education on Safe Mining of Deep Metal Mines, Northeastern University, Shenyang 110819, China

[3] University of Chinese Academy of Sciences, Beijing 100049, China

Based on a true triaxial testing platform for complete stress–strain process of hard rock (Feng et al. 2016), a series of the true triaxial compression tests under different stresses were carried out on a total of 41 marble specimens from the CJPL-II to investigate their strength and deformation characteristics, with particular interest in the residual strength.

2 Testing

2.1 Specimens and Test System

The sample is a thick-layer, fine-grain white marble with single lithology, taken from the CJPL-II. The average density is 2.82 g/cm^3 and major mineral components contain dolomite and calcite. According to the ISRM suggested method (Fairhurst and Hudson 1999), specimens were made into cuboids measuring 50 mm × 50 mm × 100 mm, with a tolerance of ±0.02 mm and a maximum vertical deviation of ±0.01 mm.

The true triaxial system was established by Northeastern University, China (Feng et al. 2016; Kong et al. 2018). The stiffness of loading framework of the system along the σ_1 direction is 6 MN/mm (higher than the suggested value of 5 MN/mm (Fairhurst and Hudson 1999)). By applying a closed-loop servo-controlled system with extremely rapid and flexible servo valve, the post-peak deformation and failure of rock can be controlled to allow acquisition of the complete stress–strain curve and residual strength. Additionally, the system was equipped with the PCI-2 acoustic emission (AE) monitoring device from the US Physical Acoustics Corporation.

2.2 Test Scheme and Loading Stress Paths

The CJPL-II was constructed in a deep zone with high geostress (σ_3, σ_2, and σ_1 of about 25, 67, and 69 MPa, respectively). The surrounding rocks experience complex redistribution of 3D stress after excavation. Therefore, it is necessary to conduct true triaxial compression under 3D stress state (σ_3, σ_2): σ_3 and σ_2 are between 0 and 50 MPa, and 0 to 200 MPa, respectively. The test scheme and stress levels are summarised in Table 1.

The stress paths during true triaxial compression are illustrated in Fig. 1 and the main loading steps are shown as follows:

1) The hydrostatic pressure ($\sigma_1 = \sigma_2 = \sigma_3$) was applied at a constant rate of 0.5 MPa/s to the set value;
2) Keeping σ_3 unchanged, σ_1 and σ_2 were synchronously increased at the same rate of 0.5 MPa/s to the set values;

Table 1 Experimental results of the CJPL-II marble under true triaxial compression

Number	σ_3 (MPa)	σ_2 (MPa)	σ_c (MPa)	$\varepsilon_{c\,(\%)}$	σ_{r0} (MPa)	$\varepsilon_{r0\,(\%)}$	Number	σ_3 (MPa)	σ_2 (MPa)	σ_c (MPa)	$\varepsilon_{c\,(\%)}$	σ_{r0} (MPa)	$\varepsilon_{r0\,(\%)}$
N.1	0	0	192	0.42	–	–	N.22	15	200	377	0.65	–	–
N.2	1	30	233	0.57	–	–	N.23	20	20	295	1.21	171	2.57
N.3	2	2	202	0.43	54	0.99	N.24	20	30	311	1.15	165	2.08
N.4	2	15	195	0.49	51	0.66	N.25	20	50	341	1.01	141	1.58
N.5	2	30	223	0.62	44	0.71	N.26	20	65	369	1.10	158	1.33
N.6	2	65	233	0.45	–	–	N.27	20	100	387	0.87	177	1.07
N.7	5	5	238	0.53	73	1.96	N.28	20	135	402	0.60	179	0.88
N.8	5	15	245	0.69	65	1.22	N.29	30	30	338	1.50	225	3.25
N.9	5	30	266	0.67	61	0.90	N.30	30	40	368	1.13	216	2.01
N.10	5	50	282	0.53	–	–	N.31	30	50	385	0.95	211	1.48
N.11	5	100	310	0.48	–	–	N.31	30	65	392	0.95	208	1.89
N.12	10	10	248	0.60	102	2.27	N.33	30	80	408	0.96	194	1.50
N.13	10	30	287	0.79	94	1.49	N.34	30	105	413	1.05	192	1.54
N.14	10	65	314	0.80	87	0.97	N.35	30	120	426	1.06	214	1.55
N.15	10	100	326	0.59	–	–	N.36	30	150	441	0.89	219	1.17
N.16	15	15	264	0.76	136	2.21	N.37	40	40	386	1.86	286	3.71
N.17	15	22.5	293	0.84	125	2.08	N.38	40	50	415	1.71	–	–
N.18	15	30	299	0.89	127	1.48	N.39	40	100	460	1.31	241	1.78
N.19	15	65	334	0.68	115	1.08	N.40	40	200	512	0.96	290	1.23
N.20	15	100	352	0.66	127	0.80	N.41	50	100	479	1.21	298	1.65
N.21	15	135	368	0.73	141	0.84							

The rock is CJPL-II marble, σ_3, σ_2, σ_c, ε_c, σ_{r0} and ε_{r0} are the minimum principal stress, intermediate principal stress, peak strength and corresponding to strain, and initial residual strength and corresponding to strain, respectively; "–" denotes no data

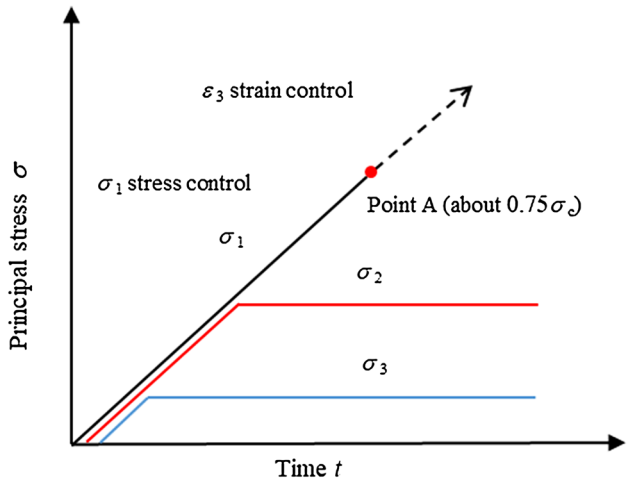

Fig. 1 True triaxial loading paths: σ_1 stress control and ε_3 strain control are applied before and after point A (about $0.75\sigma_c$), respectively

3) Keeping σ_3 and σ_2 constant, σ_1 was further increased while the strain rate in the ε_3-direction was measured. When the rate reached 0.5×10^{-5} (point A, about 75% of peak strength σ_c), the control mode for σ_1 was changed to strain control along the ε_3 direction. Moreover, σ_1 was further applied at the constant ε_3 strain rate until the residual strength of rock was mobilised.

3 Test Results and Analysis

3.1 Characteristics of the Complete Stress–Strain Curve Under True Triaxial Compression

Figure 2 shows several typical complete stress–strain curves (deviatoric stress versus strain in three directions) of marble under true triaxial compression. When $\sigma_3=\sigma_2$, these are relatively smooth post-peak curves. With increasing σ_2 or decreasing σ_3, multiple stress drops appear in the post-peak stage, as found elsewhere (Mogi 1973) that brittle failure was accompanied by a marked stress drop. Here, the stress drops do not refer to sudden uncontrollable stress drops (Wawersik and Brace 1971; Hudson et al. 1972), but the servo-controlled stress drops match crack-induced brittle failure in rock. In the failure state, the peak strength and residual strength can thus be investigated.

The test results of all specimens are listed in Table 1. Mechanical properties of rock are then derived from the stress–strain curve, as shown in Fig. 3. σ_c refers to the peak strength, ε_c is the peak strain corresponding to σ_c, σ_{r0} is defined as the initial residual strength when the rock just enters its residual stage, and ε_{r0} is the strain corresponding to σ_{r0}. Subsequent deformation along the ε_1-direction is defined as residual slip deformation X. As the residual strength significantly decreases with X, $\Delta\sigma_r$ is the reduction of residual strength relative to σ_{r0}. Determination of σ_{r0} has definite physical meaning: Fig. 3 shows that the point at $\sigma_1=\sigma_{r0}$ is the sharp turning point in the complete stress–strain curve from the post-peak brittle failure stage to the residual stage. AE activity is significantly different before and after this point. Furthermore, the failure mechanisms of the two stages are also obviously different. The former mainly involves the propagation and coalescence of microcracks and local cracks inside rock, resulting in a through-fractured surface, while the latter is mainly the local rupture of asperities on the failure surfaces. Therefore, σ_{r0} is considered to be the strength of the failed rock that has just formed a through-fractured surface under true triaxial compression.

3.2 Peak Strength Characteristics Under True Triaxial Compression

Figure 4 shows the peak strength characteristics of marble in different stress states under true triaxial compression. It can be seen that σ_2 has a significant effect on peak strength (σ_c). For each tested σ_3, σ_c increases with σ_2 at a gradually decreasing rate, until a plateau is reached at some σ_2 value, which conforms to previous conclusions (Mogi 1971; Ma and Haimson 2016; Zhao et al. 2018). In the test, σ_2 is not large enough to result in a decline in σ_c, but it satisfies engineering requirements.

4 Residual Strength of Marble Under True Triaxial Compression

4.1 Deformation-Dependence on Residual Strength and Its AE Characteristics

By carrying out conventional triaxial compression, some scholars (Wawersik and Brace 1971; Cai et al. 2007a; Peng et al. 2017) suggested that residual strength of rock shows deformation-dependence, gradually declining with increasing deformation in residual stage. However, there are few test results showing the complete stress–strain curves under true triaxial compression at present and therefore investigating the deformation-dependent residual strength of marble under 3D stress state and its AE characteristics are novel.

Figure 2 also demonstrates the relationships of σ_1–σ_3 with ε_1, ε_2, and ε_3 in the residual stage. The deformation along the ε_1 and ε_3-directions constantly increases whether the residual strength decreases or not. Under true triaxial stresses ($\sigma_2>\sigma_3$), the deformation along the ε_2-direction does not increase when the residual strength decreases, which is different from that in conventional triaxial stresses ($\sigma_2=\sigma_3$). Because when $\sigma_2>\sigma_3$, the failure surfaces which have been formed before the residual stage are parallel to σ_2 in the

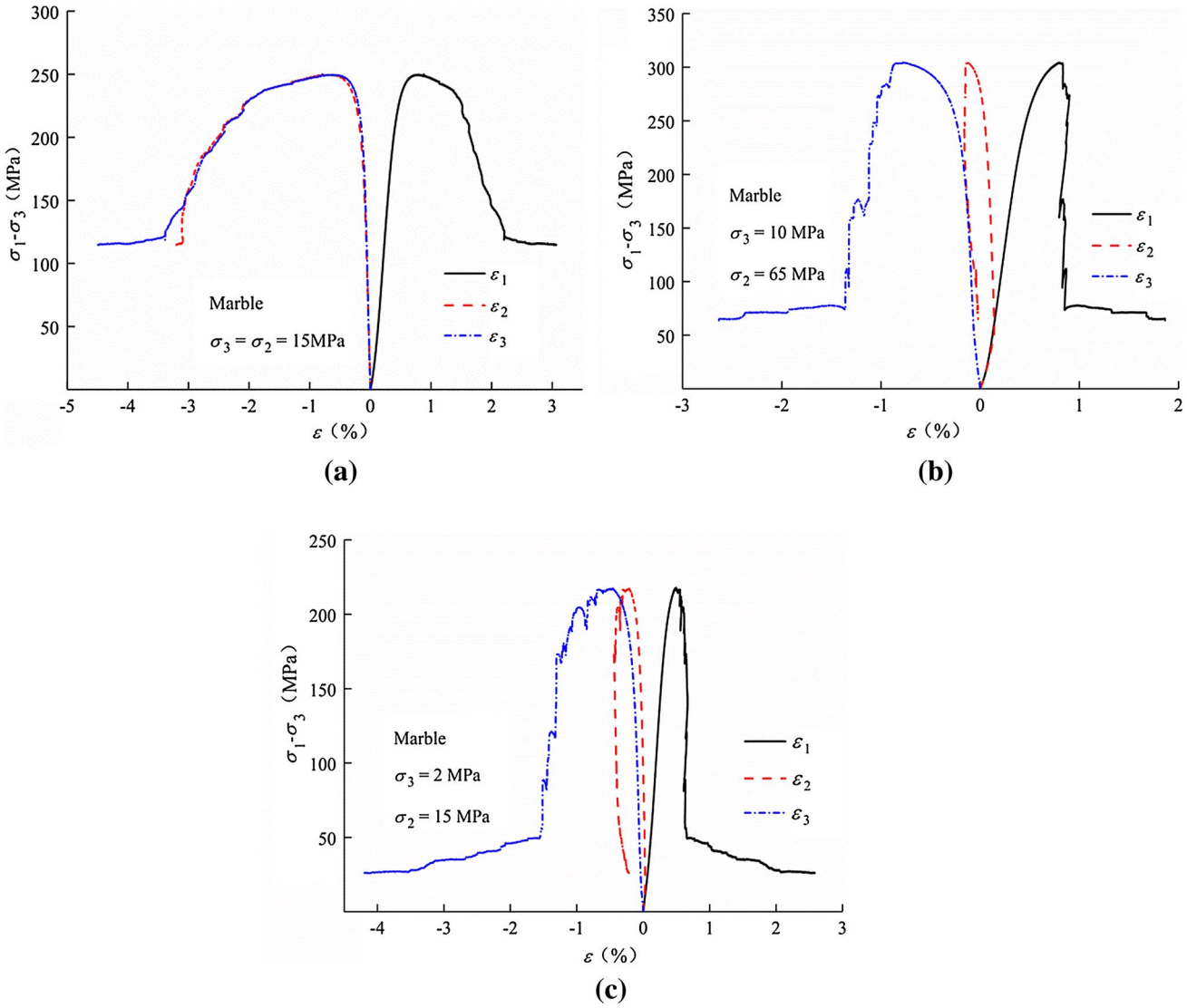

Fig. 2 Typical complete stress–strain curves of CJPL-II marble under true triaxial compression: **a** curves in conventional triaxial stress states ($\sigma_2 = \sigma_3$); **b** and **c** curves in true triaxial stress states ($\sigma_2 > \sigma_3$)

σ_1–σ_3 plane (Fig. 7). This is in accordance with previous conclusions (Mogi 1973; Ma and Haimson 2016). Therefore, during slip along the failure surface, deformation along the directions of σ_1 and σ_3 significantly increases while that along the direction of σ_2 only evinces the elastic rebound caused by reduction in σ_1.

To show deformation-dependence of residual strength, several typical curves of the variations of residual strength with X are displayed in Fig. 5a. It can be seen that the residual strength of marble is subjected to multiple reductions at small amplitude with increasing X. A quantitative description of this reduction is given in Fig. 5b, which reveals the relationship between $\Delta\sigma_r/\sigma_{r0}$ and $\varepsilon_1/\varepsilon_c$. As the deformation increases, the residual strength significantly decreases compared with σ_{r0}. For example, the value of $\Delta\sigma_r/\sigma_{r0}$ corresponding to $\varepsilon_1/\varepsilon_c = 5.2$ at $\sigma_3 = 2$ MPa and $\sigma_2 = 15$ MPa reaches 45.2%, which is still not the final value. Therefore, the residual strength shows significant deformation-dependence in 3D stress states.

Figure 6 reveals AE characteristics in the residual stage at $\sigma_3 = 2$ MPa and $\sigma_2 = 15$ MPa. The AE count rate is low and when failure reaches the stress reductions, AE activity increases and the AE count rate matches the rate of σ_1 decrease. From Fig. 7a, it can be seen that the failure surface is not a simple plane but one with significant asperities. After undergoing significant slip deformation, the failure plane with obvious asperities may show local crushing and even contain secondary fractured surfaces probably due to frictional effects (Fig. 7b), resulting in

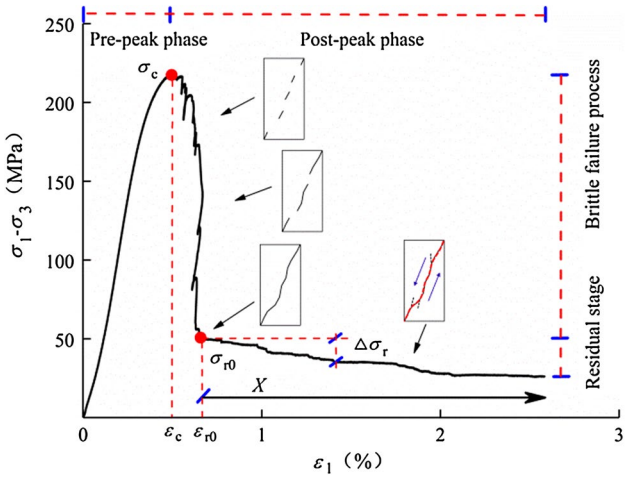

Fig. 3 Determination of peak strength σ_c and corresponding to strain ε_c, initial residual strength σ_{r0} and corresponding to strain ε_{r0}, and residual slip deformation X, reduction of residual strength $\Delta\sigma_r$ from the complete stress–strain curve

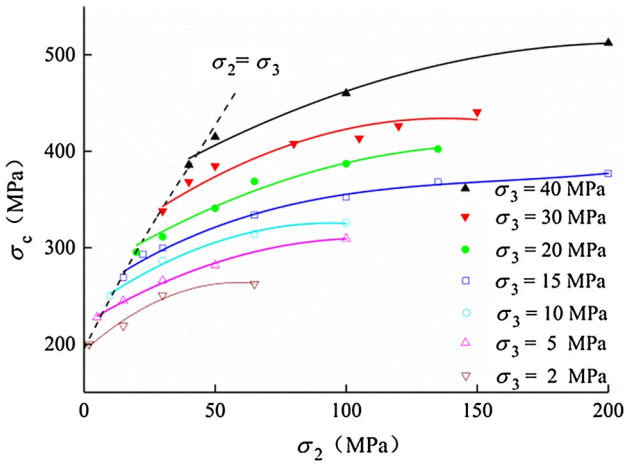

Fig. 4 Peak strength characteristics of the CJPL-II marble under true triaxial compression. The solid lines show the trend line of peak strength and the best-fit polynomial

generation of strengthened AE signals as well as corresponding reductions in residual strength.

4.2 The Influence of σ_3 on Residual Strength

As an absolutely stable residual strength cannot be truly acquired by laboratory testing due to deformation-dependence, there is no universal definition of residual strength at present (Cai et al. 2007a; Gao and Kang 2017; Peng et al. 2017). Therefore, σ_{r0} owing to the obvious physical meaning (as explained in Sect. 3.2), can be investigated under true triaxial compression. The residual strength mentioned below also refers to this value.

There has been much research on residual strength under conventional triaxial stress conditions, which was consistent with the Mohr–Coulomb or Hoek–Brown criteria. In Fig. 8a, the residual strength data at $\sigma_3 = \sigma_2$ were fitted by the linear Mohr–Coulomb strength criterion:

$$\sigma_{r0} = a\,\sigma_3 + b, \tag{1}$$

where a and b are constants, which are related to the cohesion c and internal friction angle φ, and can be expressed as follows:

$$a = (1+\sin\varphi)/(1-\sin\varphi),\ b = (2c\cos\varphi)/(1-\sin\varphi). \tag{2}$$

Table 2 displays the fitting result. The linear correlation coefficient R^2 between the residual strength and confining pressures at $\sigma_3 = \sigma_2$ is 99.8%, thus evincing high conformance with the Mohr–Coulomb criterion, which is consistent with previous scholars' conclusions (Cai et al. 2007a, b; Yang et al. 2012). However, this is the residual strength characteristics at $\sigma_3 = \sigma_2$. After excavation of deep underground caverns, σ_3 gradually decreases from geostress level in primitive rock zone to near zero at the free face, while the variation of σ_2 is not synchronous with that of σ_3. Therefore, it is necessary to evaluate the contribution of independent σ_3 and σ_2 to residual strength, respectively.

Figure 8b reveals the variation of σ_{r0} with σ_3 for each constant value of σ_2. The residual strength obtained for different σ_3 at a given σ_2 was also fitted by linear Mohr–Coulomb criterion. The fitting results show that residual strength exhibits a favourable linear relationship as all the R^2 exceed 98.1%. When σ_2 is 15 MPa, 30 MPa, 65 MPa, and 100 MPa, the corresponding values of a are 6.713, 6.660, 6.139, and 4.571, respectively, decreasing with increasing σ_2, which decreases the effect of σ_3 on increasing residual strength.

The effect of σ_3 on residual strength parameters (cohesion c and internal friction angle φ) is evaluated for each constant σ_2, by examining the corresponding values at that σ_2 with its magnitude when $\sigma_2 = \sigma_3$ (Table 2). When $\sigma_2 \le 65$ MPa, the internal friction angle for a given σ_3 is slightly larger than that when $\sigma_3 = \sigma_2$ while the cohesion exhibits the opposite trend. When $\sigma_2 > 65$ MPa, the internal friction angle is slightly smaller than that when $\sigma_3 = \sigma_2$ while the opposite applies to the cohesion.

4.3 The Influence of σ_2 on Residual Strength

As shown in Table 1 and Fig. 9a, σ_2 exhibits a certain influence on residual strength in true triaxial stresses. Although the influence is inferior to the effect of σ_3, it shows certain regularity. To study the σ_2 effect and conveniently conduct a comparison with the result under conventional triaxial stresses, a new coefficient u_i for residual strength is defined:

$$u_i = (\sigma_{rij} - \sigma_{ric})/\sigma_{ric}, \tag{3}$$

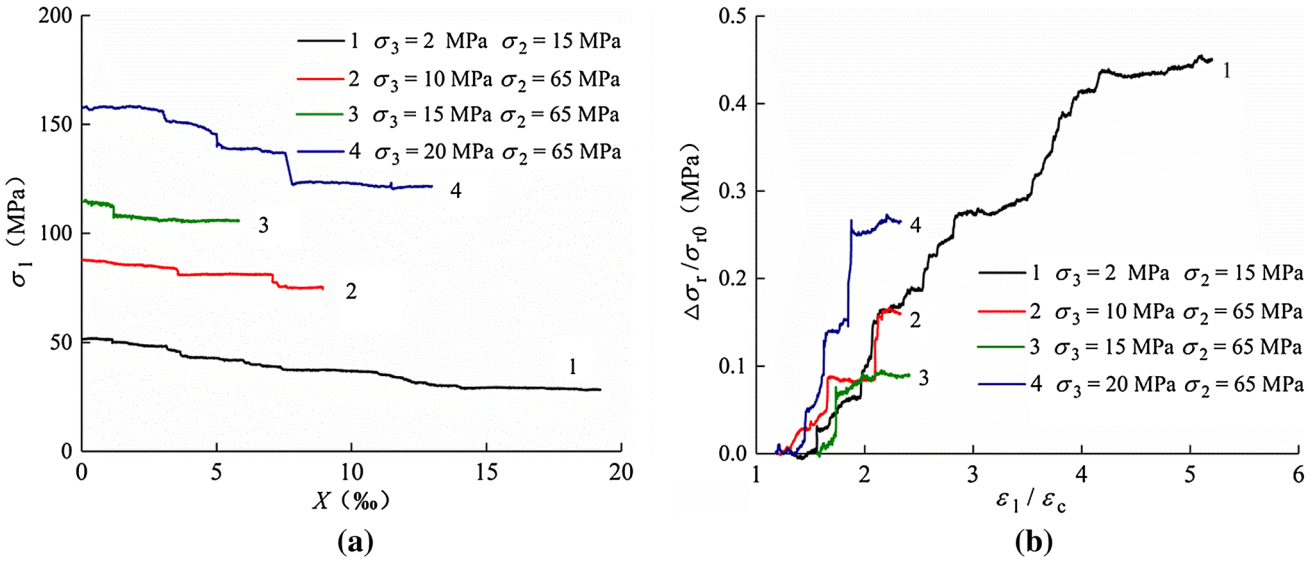

Fig. 5 Deformation-dependent residual strength of marble in several typical 3D stress states: **a** variation of residual strength with residual slip displacement X; **b** the relationship between $\Delta\sigma_r/\sigma_{r0}$ and $\varepsilon_1/\varepsilon_c$

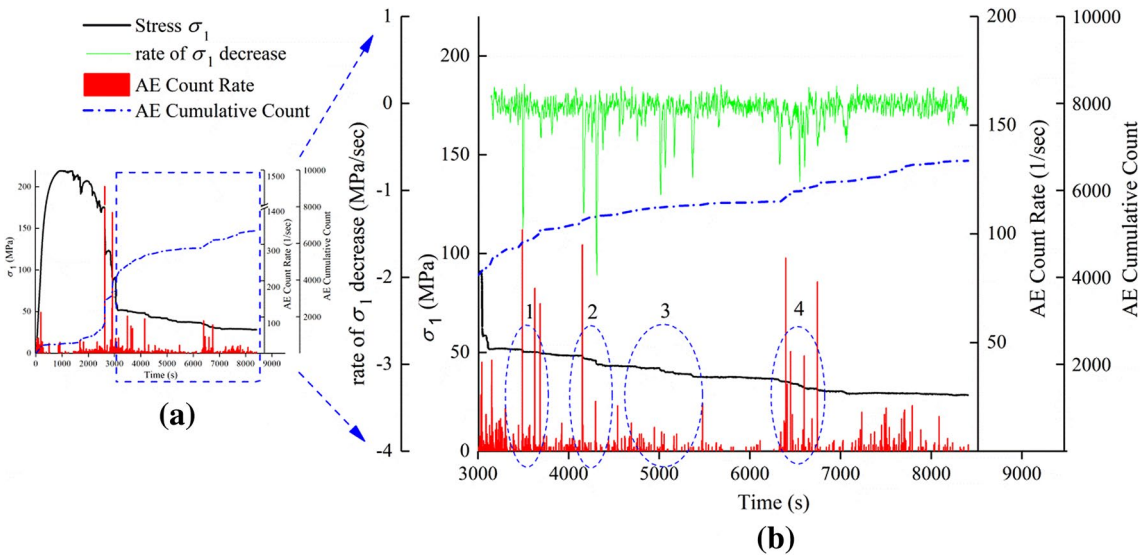

Fig. 6 AE characteristics in the residual stage at $\sigma_3 = 2$ MPa and $\sigma_2 = 15$ MPa. 1, 2, 3, and 4 represent the first, second, third, and fourth stress reductions, respectively

where σ_{tic} and σ_{tij} represent the residual strength in conventional and true triaxial stresses, respectively. When $\sigma_2 = \sigma_3$, $u_i = 0$.

It can be seen from Fig. 9b that u_i varies with σ_2. For a high σ_3 (> 10 MPa), coefficient u_i significantly decreases from zero to a low value at some σ_2 value with increasing σ_2, then returns to near-zero values. For a low σ_3 (≤ 10 MPa), u_i decreases with increasing σ_2. The lowest values of u_i at $\sigma_3 = 2$, 5, 10, 15, 20, 30, and 40 MPa are −0.178, −0.163, −0.147, −0.174, −0.136, and −0.157, respectively.

In other words, the residual strength of marble exerts a certain σ_2 effect. It decreases at first and then increases with σ_2 for a high σ_3 while declining with σ_2 for a low σ_3. It is worth noting that the residual strength in true triaxial stress states is generally lower (by 13.6–17.8% at most) than that in conventional triaxial stresses at the same σ_3. The reasons for the σ_2 effect on residual strength of marble will be analysed in Sect. 5.1.

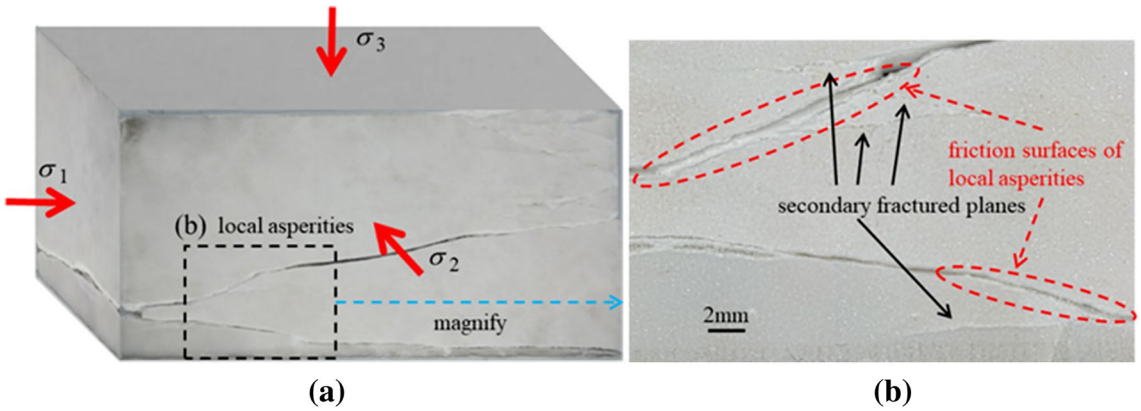

Fig. 7 Macroscopic failure morphology under true triaxial compression at $\sigma_3 = 2$ MPa and $\sigma_2 = 15$ MPa: **a** the failed marble specimen photograph; **b** optical microscopy observation (magnified ×30)

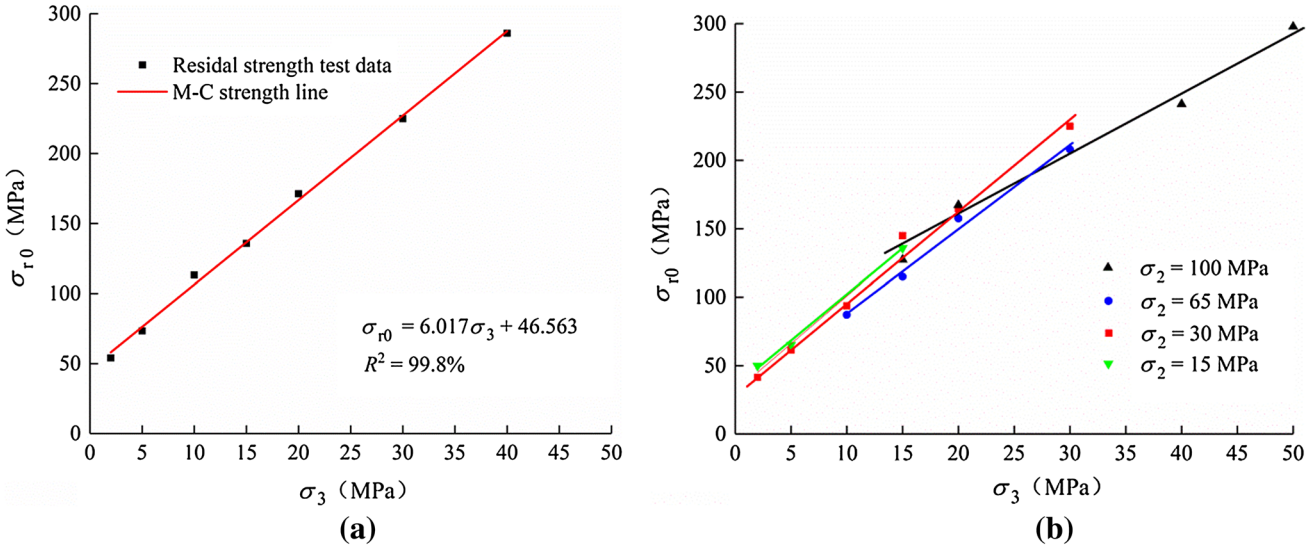

Fig. 8 The relationship between the residual strength σ_{r0} and σ_3: **a** test values of residual strength at $\sigma_2 = \sigma_3$ and predicted values based on the M–C strength criterion; **b** variation of σ_{r0} with σ_3 at $\sigma_2 = 15$, 30, 65, and 100 MPa

Table 2 Linear fitting result between σ_{r0} and σ_3

Stress states (MPa)	*a*	*b*	*c* (MPa)	φ (°)	R^2
$\sigma_2 = \sigma_3$	6.017	46.563	9.49	45.64	99.8%
σ_2					
15	6.713	34.443	6.65	47.79	99.4%
30	6.660	30.871	5.98	47.64	98.7%
65	6.139	26.800	5.41	46.04	98.9%
100	4.571	65.556	15.33	39.87	98.1%

c cohesion, φ frictional angle, R^2 the linear correlation coefficient

5 Discussion

5.1 Causal Analysis of σ_2 Effect on Residual Strength

When rock enters its residual stage, the macroscopic through-fractured surfaces have formed and the frictional resistance related to the characteristics of failure surfaces greatly determines residual strength (Cai et al. 2007a; Liang et al. 2017). Figure 10 shows that the failure morphology varies with σ_2 at the same σ_3, which is not a simple plane but one with obvious asperities and multiple fractures. The σ_2 effect on residual strength may relate to the variation of the morphology of fractures with

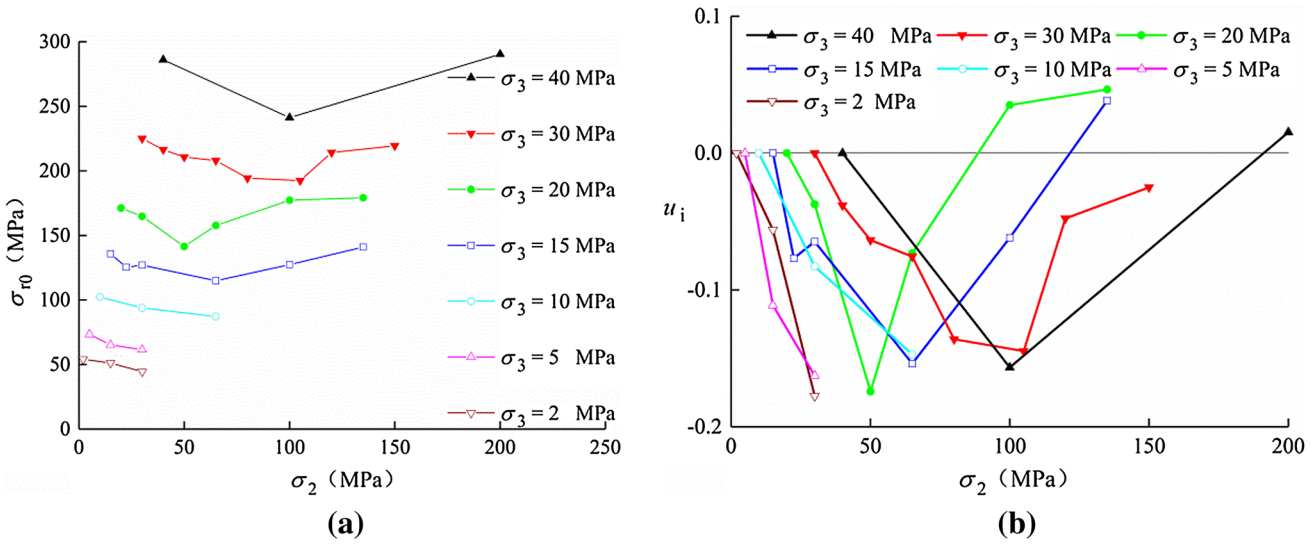

Fig. 9 The σ_2 effect on residual strength. **a** The relationship between residual strength σ_{r0} and σ_2; **b** variation of u_i with σ_2 for each constant σ_3 value

σ_2. Taking stress states such as different σ_2 at $\sigma_3 = 30$ and 40 MPa as typical examples of high σ_3 although they cannot represent all conditions. The morphology can be approximately divided into two types: one is the composite of a primary fracture and V-shaped secondary fractures (Fig. 10a, c, d, f), the other is a single primary fracture (Fig. 10d) or single primary fracture trend (Fig. 10b). For low σ_2 at $\sigma_3 = 30$ and 40 MPa, the failure morphology is of the composite type. With increasing σ_2, the morphology evolves into the single type at some σ_2 value, and then returns to the composite type. In terms of the composite type, the residual strength is high, not only including frictional resistance along the primary fracture but also that along V-shaped secondary fractures and corresponding mechanical resistance to embedment. For the single type, the residual strength only includes frictional resistance along the single primary fracture, resulting in a lower residual strength.

5.2 The Influence of Residual Strength Under 3D Stress States on the Stability of Deep Caverns

Cai et al. (2007a) and Yu et al. (2013) suggested that the weakening of residual strength can enlarge the EDZ after tunnel excavation by using numerical methods. Tiwari and Latha (2017) found that the influence of uncertainty of residual strength parameters on engineering safety sensitivity is greater than that of peak strength parameters. The value of σ_3 gradually decreases from the primary rock zone to free faces after deep underground cavern excavation. Timeous strengthening support installation is conducive to increasing σ_3, especially for free faces nearby, which can rapidly elevate the residual strength to thus strengthen the bearing capacity of surrounding rocks and reduce the range of the EDZ. However, the residual strength shows an obvious σ_2 effect, resulting in a reduction thereof compared with that in the conventional triaxial stresses in general, and a significant deformation-dependence. The malign influence of the two effects on residual strength, not considered in aforementioned numerical analysis of tunnels excavation, should be taken into account in analysis of the EDZ of deep caverns. The research further improves recognition of strength of the failed rock, which is significant when controlling damage to surrounding rocks and designing rock-support schemes.

6 Concluding Remarks

A series of true triaxial compression tests were carried out on the CJPL-II marble, aimed at obtaining the complete stress–strain curves (including post-peak phase) and then investigating the peak strength, especially residual strength characteristics. The residual strength under 3D stress states was provided. The deformation-dependence and influence of dependent σ_3 on residual strength were explored. Moreover, its σ_2 effect was innovatively revealed. The main conclusions are as follows:

1. The residual strength in true triaxial stress states exhibits significant deformation-dependence and multiple small-amplitude reductions as the residual deformation increases. During these reductions, AE count rates increase, which may be related to the local rupture of asperities on the failure surfaces.

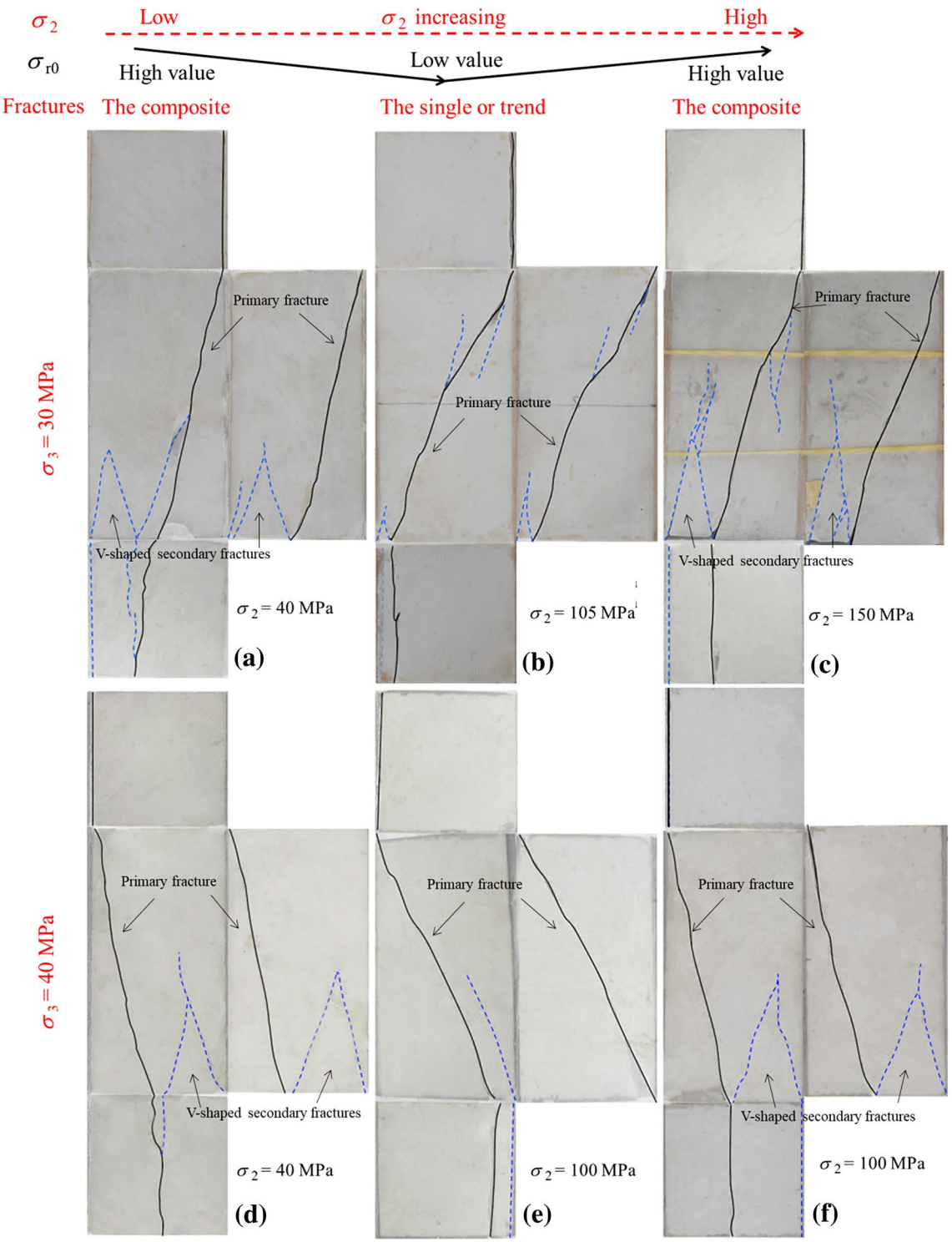

Fig. 10 Macroscopic failure morphology of marble under true triaxial compression with different σ_2 at $\sigma_3 = 30$ MPa (**a**–**c**) and 40 MPa (**d**–**f**). The black solid lines show the primary fractures, and the blue dashed lines show the secondary fractures. **a, c, d, f** are the composite of a primary fracture and V-shaped secondary fractures; **b, e** represent the single primary fracture or trend

2. The residual strength of marble shows a significant σ_3 effect, increasing linearly with σ_3 at the same value of σ_2. The residual strength also displays a certain σ_2 effect. It decreases at first and then increases with increasing σ_2 for a high given σ_3 while gradually declining with σ_2 for a low given σ_3. Therefore, the residual strength in

true triaxial stresses is generally lower (by 13.6–17.8% at most) than that in conventional triaxial stresses at the same σ_3. The σ_2 effect may be related to the variations of morphology of failure surfaces with σ_2.

3. The deformation-dependence and σ_2 effect on the residual strength of rock should be taken into account in engineering analysis and design. Otherwise, the residual strength may be over-estimated, resulting in increasing risk to safe engineering operations.

Acknowledgements The authors acknowledge the financial support from the National Key R&D Programme of China under Grant No. 2017YFC0804203, the 111 Project under Grant No. B17009, the CAS Key Research Programme of Frontier Sciences under Grant no. QYZDJ-SSW-DQC016 and the National Natural Science Foundation of China under Grant no. 51579043.

References

Al-Ajmi AM, Zimmerman RW (2005) Relation between the Mogi and the Coulomb failure criteria. Int J Rock Mech Min Sci 42:431–439

Barla G, Barla M, Debernardi D (2010) New triaxial apparatus for rocks. Rock Mech Rock Eng 43:225–230

Cai M, Kaiser PK, Tasaka Y, Minami M (2007a) Determination of residual strength parameters of jointed rock masses using the GSI system. Int J Rock Mech Min Sci 44:247–265

Cai M, Kaiser PK, Tasaka Y, Minami M (2007b) Peak and residual strengths of jointed rock masses and their determination for engineering design. In: Proceedings of the 1st Canada-US rock mechanics symposium, Vancouver, Canada, pp 259–267

Fairhurst CE, Hudson JA (1999) Draft ISRM suggested method for the complete stress–strain curve for intact rock in uniaxial compression. Int J Rock Mech Min Sci Geomech Abstr 36:281–289

Fang Z, Harrison JP (2001) A mechanical degradation index for rock. Int J Rock Mech Min Sci 38:1193–1199

Feng XT, Zhang XW, Kong R, Wang G (2016) A novel Mogi type true triaxial testing apparatus and its use to obtain complete stress–strain curves of hard rocks. Rock Mech Rock Eng 49:1649–1662

Feng XT et al (2018) In situ observation of rock spalling in the deep tunnels of the China Jinping underground laboratory (2400 m Depth). Rock Mech Rock Eng 51:1193–1213

Gao F, Kang H (2017) Experimental study on the residual strength of coal under low confinement. Rock Mech Rock Eng 50:285–296

Hashiba K, Okubo S, Fukui K (2006) A new testing method for investigating the loading rate dependency of peak and residual rock strength. Int J Rock Mech Min Sci 43:894–904

He MC, Zhao F, Cai M, Du S (2015) A novel experimental technique to simulate pillar burst in laboratory. Rock Mech Rock Eng 48:1833–1848

Hoek E, Kaiser PK, Bawden WF (1995) Support of underground excavations in hard rock. Balkema, Rotterdam

Hudson JA (1989) Rock mechanics principles in engineering practice. Butterworth-Heinemann, London

Hudson JA, Crouch SL, Fairhurst C (1972) Soft, stiff and servo-controlled testing machines: a review with reference to rock failure. Eng Geol 6:155–189

Joseph TG (2000) Estimation of the post-failure stiffness of rock. PhD Thesis. Alberta, Canada: University of Alberta

Kaiser PK (2016) Underground rock engineering to match the rock's behaviour. In: Proceedings of the 50th US Rock Mechanics / Geomechanics Symposium, Houston, Texas, USA. https://www.mirarco.org/wp-content/uploads/mirarco_pkk/MTS-Kaiser-ARMA-160526f.pdf

Kong R, Feng XT, Zhang XW, Yang CX (2018) Study on crack initiation and damage stress in sandstone under true triaxial compression. Int J Rock Mech Min Sci 106:117–123

Labuz JF, Dai ST (2000) Residual strength and fracture energy from plane-strain testing. J Geotech Geoenviron Eng 126:882–889

Li X, Feng F, Li D, Du K, Ranjith PG, Rostami J (2018) Failure characteristics of granite influenced by sample height-to-width ratios and intermediate principal stress under true-triaxial unloading conditions. Rock Mech Rock Eng 51:1321–1345

Liang Y, Li Q, Gu Y, Zou Q (2017) Experimental study on characteristics of post-peak residual strength and fracture surface of shale under various confining pressures. Chin J Min Saf Eng 34:1179–1185 (**in Chinese**)

Liao JJ, Hsieh HY (1999) Triaxial residual strength of an anisotropic rock. In: Proceedings of 37th US Rock Mechanics Symposium (Vail Rocks 99), VAIL, CO, pp 317–327

Ma XD, Haimson BC (2016) Failure characteristics of two porous sandstones subjected to true triaxial stresses. J Geophys Res 121:6477–6498

Mogi K (1971) Fracture and flow of rocks under high triaxial compression. J Geophys Res 76:1255–1269

Mogi K (1973) Rock fracture. Annu Rev Earth pl Sci, 1:63–84

Peng J, Cai M, Rong G, Yao MD, Jiang QH, Zhou CB (2017) Determination of confinement and plastic strain dependent post-peak strength of intact rocks. Eng Geol 218:187–196

Su G et al (2017) True triaxial experimental study of rockbursts induced by ramp and cyclic dynamic disturbances. Rock Mech Rock Eng 51:1027–1045

Tiwari G, Latha GM (2017) Reliability analysis of jointed rock slope considering uncertainty in peak and residual strength parameters. Bull Eng Geol Environ 11:1–18

Wawersik WR, Brace WF (1971) Post-failure behavior of a granite and diabase. Rock Mech 3(2):61–85

Yang SQ, Jing HW, Wang SY (2012) Experimental investigation on the strength, deformability, failure behavior and acoustic emission locations of red sandstone under triaxial compression. Rock Mech Rock Eng 45:583–606

Yu W, Xiao LI, Shouding LI, Hou W, Wu YS, Bo Z (2013) A method for determining residual strength parameters of jointed rock masses. Chin J Rock Mech Eng 32:1701–1713 (**in Chinese**)

Zhang CH, Zhao QS, Li H, Sen YE, Yu YJ (2010) Post-peak strain softening mechanical model of rock considering confining pressure effect. Chin J Rock Soil Mech 31:193–197 (**in Chinese**)

Zhao J, Feng XT, Zhang XW, Zhang Y, Zhou YY, Yang CX (2018) Brittle-ductile transition and failure mechanism of Jinping marble under true triaxial compression. Eng Geol 232:160–170